Nr 9 (595–664) WRZESIEŃ 2020 Tom LXV

POLIMERY

Study of alkanethiol-based self-assembled monolayers coated with poly(methyl methacrylate) of various tacticity*)

Tomasz Kozik[1), **)], Maciej Śniechowski[1)], Wojciech Łużny[1)]

DOI: dx.doi.org/10.14314/polimery.2020.9.1

Abstract: Self-assembled monolayers (SAMs) have a large variety of applications. One particular application of alkanethiol-based SAMs is tuning the work function of metallic surfaces. In a recent study, it was determined that depositing a poly(methyl methacrylate) layer on selected SAMs further shifts the work function. The effect is sensitive to tacticity and neither the reason behind this nor the exact mechanism of the interaction was determined. The aim of this work is to study the problem by use of molecular dynamics simulations.

Keywords: self-assembled monolayers, poly(methyl methacrylate), molecular dynamics.

Badanie samoorganizujących się monowarstw na bazie alkanotioli pokrytych poli(metakrylanem metylu) o różnej taktyczności

Streszczenie: Jednym z licznych zastosowań samoorganizujących się monowarstw (SAMs) jest modyfikacja pracy wyjścia powierzchni metalicznych. W literaturze można znaleźć opracowania dotyczące depozycji cienkich warstw poli(metakrylanu metylu) na wybranych samoorganizujących się monowarstwach na bazie alkanotioli, prowadzącej do dalszych zmian wartości pracy wyjścia całej struktury. Uzyskany efekt wydaje się być zależny od taktyczności polimeru, jednakże w badaniach eksperymentalnych nie udało się określić przyczyn tego zjawiska. W niniejszej pracy wspomniany efekt zbadano za pomocą symulacji komputerowych metodą dynamiki molekularnej.

Słowa kluczowe: samoorganizujące się monowarstwy, poli(metakrylan metylu), dynamika molekularna.

Self-assembled monolayers, commonly abbreviated SAMs, are some of the most simple systems in which the process of self-assembly occurs [1]. Essentially, the self-assembly process is the spontaneous formation of large, ordered structures by simple molecules, in the case of SAMs during adsorption on metallic surfaces. Molecules capable of forming SAMs have typically the form of a backbone separating a head group and a tail group. SAMs are very important structures in nanotechnological applications, since they can be used as general metal-organic interfaces and deposited on surfaces of metallic nanoparticles or metallic surfaces. Apart from protective applications, metallic surfaces and nanoparticles may be functionalized by SAMs, depending on the form of the terminal group. One application of such functionalized surfaces are biosensor chips for Surface Plasmon Resonance (SPR) measurements [2].

[1)] AGH University of Science and Technology, Faculty of Physics and Applied Computer Science, al. Adama Mickiewicza 30, 30-059 Krakow, Poland.

*) Material contained in this article was presented at the XI International Conference on "X-ray Investigations of Polymer Structure", 3–6 December 2019, Ustroń, Poland.

**) Author for correspondence: Tomasz.Kozik@fis.agh.edu.pl

SAMs, in particular alkanethiol-based ones, affect the work function of the surface they are deposited on. Such an effect is observed in theoretical studies [3–5] as well as experimental ones [6]. In the latter paper, SAMs formed by hexadecanethiol and 1-mercapto hexadecanoic acid on the gold (111) surface were coated with poly(methyl methacrylate), PMMA. It was determined that this introduces a further work function shift, which could have several applications. Intriguingly, the effect is sensitive to the tacticity of the PMMA. The reason behind this is unknown.

The aim of this work is to determine the mechanism of interaction between the two mentioned types of SAMs with PMMA, the effect of the interaction and how the effect depends on the tacticity of the polymer. The primary means of study was molecular dynamics simulations of the studied systems.

EXPERIMENTAL PART

Molecular dynamics simulations

Molecular dynamics simulations performed in this work were carried out in the simulation package GROMACS [7–12]. The general purpose OPLS-AA force field was used [13–20]. The internal residue database of the simulation package was complemented with models of SAM-forming molecules and PMMA mers, which is discussed in more detail in subsequent chapters. Partial charge models for SAMs were based on DFT [21, 22] calculations using the 6-31G* Gaussian orbital basis set [23] with the B3LYP exchange-correlation potential [24, 25] performed in the NWChem package [26]. Visualizations of molecular dynamics frames were prepared using VMD [27].

Models of CH_3-terminated and COOH-terminated SAMs

For simulating a CH_3-terminated SAM, a model of hexadecanethiol stripped of the hydrogen atom from the thiol group and complemented with three gold atoms closest to the preferred adsorption site of sulfur was added to the internal residue database of GROMACS. The partial charges in this model were based on DFT calculations for an isolated hexadecanethiol molecule. All necessary potentials for such a residue were already included in the OPLS-AA force field, with the exception of potentials involving gold atoms. Three additional Morse type bond potentials between the sulfur atom and each of the three gold atoms were introduced to account for adsorption. The parameters of the bond potential were obtained by fitting their values to reproduce near the adsorption site the potential calculated by Zhang *et al*. [28]. This was deemed appropriate, as the molecule would not leave the vicinity of this site in the course of the simulation.

A fully analogous model of a 1-mercapto hexadecanoic acid SAM was used.

The essential models of both SAMs were built as arrays of 20 × 20 molecules, with the sulfur atoms forming an ideal hexagonal surface structure, corresponding to the characteristic $(\sqrt{3} \times \sqrt{3})$ R30 SAM structure [29]. The resulting horizontal simulation box dimensions were approximately 9.99 nm by 8.65 nm. To provide a nearly, but not entirely, rigid model of the gold (111) surface underneath the SAM, four more layers of gold atoms were added below the SAM according to the *fcc* structure of gold. The positions of atoms in the bottommost layer were fixed in all simulations. Harmonic bond potentials adapted from the work of Lincoln *et al*. [30] were applied between all gold atoms being nearest neighbors in the five layers within the model.

Equilibrated models of the two studied SAM structures were obtained by performing a Molecular Dynamics (MD) simulation of 2 000 000 steps of 1 fs. Electrostatic interactions were handled using the Particle Mesh Ewald (PME) method [31, 32] with the Verlet cut off scheme [33], with a short-range cutoff of 3.5 nm. The initial velocities of atoms were generated from a Maxwell distribution at 300 K. The temperature was controlled using a velocity rescale thermostat with a constant equal to 1. No pressure coupling was used as the simulation box had a constant volume. Afterwards, a 300 000 step simulation with 1 fs steps was performed for data collection, with output written every 1 ps.

Models of amorphous PMMA of different tacticity on top of SAMs

Instead of performing a random walk simulation to generate amorphous polymer models, a generating "die casting" simulation as described by Feenstra *et al*. [34] was adapted for generating such models.

Initial arrangements of PMMA chains of different tacticity consisted of 12 chains of 150 mers each (mass of *ca*. 15.02 kDa), generated as a very low density structure of nearly straight chains spanning a simulation box with a vertical dimension of 100 nm and horizontal dimensions adjusted to the size of the SAM. The chains were interwound via the periodic boundary conditions, but did not intersect the top and bottom boundary. The partial charge model of the PMMA mers was taken from [35]. The chains were terminated using hydrogen atoms on both ends.

For each tacticity and each type of SAM, the low density structure was placed on top of an equilibrated SAM. After generating velocities of atoms from a Maxwell distribution at 300 K, the system underwent a preliminary MD simulation of 100 000 steps of 0.5 fs each. The temperature was controlled using a velocity rescale thermostat with a constant equal to 1. For pressure coupling, the anisotropic Berendsen barostat was used to apply an arbitrarily high pressure of 50 MPa (500 bar) in the ver-

tical direction only, with a constant of 0.2. The primary purpose of this simulation was reducing the extreme disproportion between the dimensions of the box and ensuring the chains would not unwind.

Next, a modified "die casting" simulation was performed in the electrostatic field produced by the SAM. The entire SAM structure was excluded from position updates of atoms to prevent damaging it, as the aim of the simulation was to only generate an amorphous polymer structure. It took 3 500 000 steps of 1 fs each with settings similar to the ones used earlier. While maintaining a pressure of 50 MPa in the vertical direction only, the velocity rescale thermostat was used for controlling the temperature of the polymer. Due to periodic boundary conditions, the bottommost layer of gold atoms acted as a "wall" for the polymer. The temperature was coupled to 300 K for the first 100 ps of the simulation, increased linearly to an arbitrary extreme value of 1 000 K during the next 100 ps, stayed at 1 000 K for 300 ps and decreased linearly back to 300 K through a time period of 2 ns. The simulation continued in 300 K for 1 ns.

For equilibration, the vertical length of the simulation box was increased to 10 nm, to separate the system from its periodic image in this direction. 2 000 000 time steps of 1 fs each were performed, during which the SAM (except the bottommost layer of gold) was free to move again and to adjust to the formed layer. The simulation parameters were the same, except that at this point there was no need for a barostat. The temperature was coupled to 300 K using a velocity rescale thermostat.

The systems obtained in the above described simulation sequences were considered good models of amorphous polymer layers formed in the electrostatic fields of SAMs.

Finally, a simulation of 300 000 time steps of 1 fs each was performed for acquiring data in every case (tacticity versus SAM type), with output every 1 ps.

Source of experimental data

The paper by Marzec *et al*. [6] may be used as a source of data for comparing simulation results with experiment. In Kelvin Probe Force Microscopy (KPFM) measurements, the authors recorded a difference of *ca*. 270 mV in contact potential difference between a CH_3-terminated SAM and a COOH-terminated SAM, with a higher value for the former. After coating their "brick wall" structure of these two different SAMs with isotactic and syndiotactic PMMA, the measured difference changed to *ca*. 95 mV and *ca*. 100 mV, respectively. After coating with non-ideal atactic PMMA, the measured difference changed to *ca*. 30 mV, but this time a higher contact potential difference was measured for the COOH-terminated SAM.

The effect of coating with PMMA can be summarized in all cases as an increase in contact potential difference on the COOH-terminated SAM relatively to the CH_3-terminated SAM of *ca*. 175 mV, 170 mV and 300 mV for isotactic, syndiotactic and atactic PMMA, respectively.

RESULTS AND DISCUSSION

SAM models

During the relaxation simulation, both SAM models reached an equilibrium configuration. The axes of the molecules forming the CH_3-terminated SAM were tilted at an angle of (30.2 ± 1.6°) to the vertical direction and for the molecules forming the COOH-terminated SAM this angle was (31.6 ± 1.4°), based on the geometrical analysis of the final simulation frame. This was in agreement with the widely reported in literature value of *ca*. 30°. This angle is a result of packing optimization. Each molecule was leaning in the direction in between its two nearest neighboring molecules, which was in agreement with the findings by Zhang *et al*. [28]. A visualization of the final frame of the simulation for the CH_3-terminated SAM is included in Fig. 1., with the model rotated so that the SAM backbone planes are mostly perpendicular to the viewing plane.

Because both hexadecanethiol and 1-mercapto hexadecanoic acid are polar molecules, both SAMs exhibit a non-zero net electric dipole moment. The vertical components of the CH_3-terminated and COOH-terminated SAM net dipole moments μ_z were divided by the surface areas *S* of the models, to free further considerations from the impact of this choice. The obtained quantities μ_z/S were *ca*. +2.486 D/nm^2 for the CH_3-terminated SAM and *ca*. -1.05 D/nm^2 for the COOH-terminated SAM.

By considering the idealized work function shift (*WFS*) values of -1.4 eV and +1.0 eV for these SAMs, theoretically obtained by Shushko *et al*. [3–5] and applying the parallel plate capacitor model [3–5], idealized values can be calculated:

$$\mu_z/S = -\varepsilon_0 \cdot WFS/e = \varepsilon_0 \cdot V_{CPD} \quad (1)$$

This yields values of *ca*. +3.716 D/nm^2 and -2.654 D/nm^2, respectively. Comparing, the values obtained in the MD

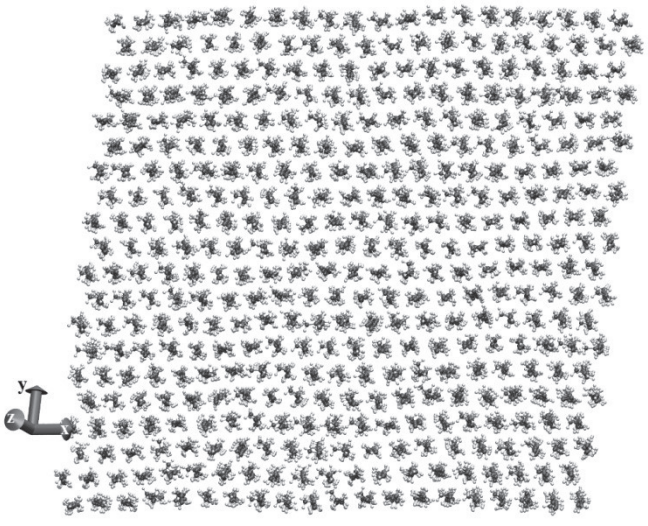

Fig. 1. The CH_3-terminated SAM model, final frame

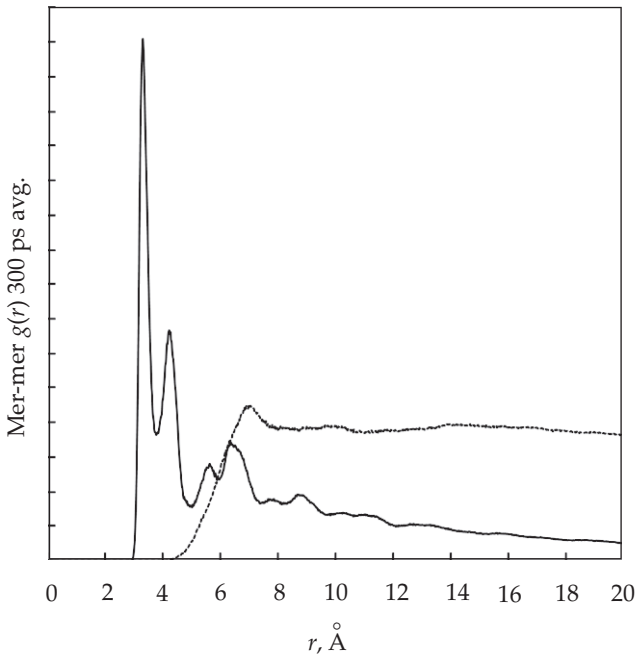

Fig. 2. The intrachain (solid) and interchain (dashed) components of the *RDF* calculated for the mer *COMs* of isotactic PMMA

simulation have a correct sign and a magnitude lower than in an idealized case, which should be expected.

The straightforward alternative form of the above equation may be applied to the value of the contact potential difference V_{CPD}. Within the framework of this model, the value resulting from the measurements of Marzec *et al*. [6] is a difference $\Delta(\mu_z/S)$ of *ca*. +0.717 D/nm^2 in favor of the CH_3-terminated SAM, while the analogous value was *ca*. +3.536 D/nm^2 in the MD simulations and is +6.37 D/nm^2 in an idealized case. This provided some insight into how non-ideal a large scale MD simulation and an experiment can be.

PMMA layers on top of SAMs

By visual investigation, the PMMA layers formed on top of the SAMs were structures of entangled chains, as desired. Whether they were truly amorphous structures was verified by calculating the time-averaged radial distribution function (*RDF*), also called pair correlation function, for the centers of mass (*COMs*) of the mers forming each polymer chain. The *RDF* was split into an intra-chain and inter-chain component, calculated for pairs belonging to the same chain and different chains respectively, and is shown in Fig. 2.

The proportion of the intensity of the first two peaks in the 3 Å to 4.5 Å range varies with tacticity. The lack of long range correlations as well as a density of the PMMA layer of between 1.12 g/cm^3 and 1.2 g/cm^3 in its bulk was considered enough of a verification that the model of the layer is proper.

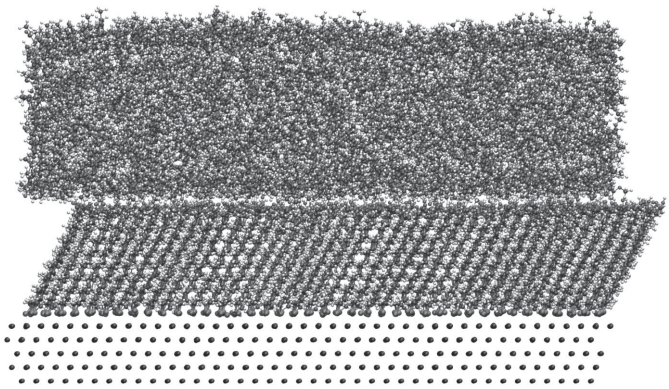

Fig. 3. Model of a PMMA layer formed on top of a CH_3-terminated SAM

Effect of interaction between PMMA and SAMs

The obtained models of amorphous PMMA layers on SAMs of two different types were analyzed to find an explanation for the mechanism of their interaction. An example of a final model, viewed from the side of the simulation box, is depicted in Fig. 3.

It was observed that the deposition of the PMMA layer does not impact the SAM itself in any way in any case. The time-averaged preferred adsorption sites of sulfur remained the *fcc* vacancy (80%) with some atoms moving closer to the *bridge* site (20%). The *atop* site was very sporadically occupied. The geometry of the SAMs, in particular the tilt angle, did not change upon depositing the polymer layer. The vertical component of the net electric dipole moment of the SAMs was also mostly unaffected.

Hydrogen bonds formed between the COOH-terminated SAM and the PMMA may be analyzed. Hydrogen bonds were designated basing on purely geometric criteria of donor-acceptor distance of at most 3.5 Å and hydrogen-donor-acceptor angle of at most 30°. Hypothetically, four principal types of hydrogen bonds may exist in the studied systems, which are schematically drawn in Formulas (I)—(IV).

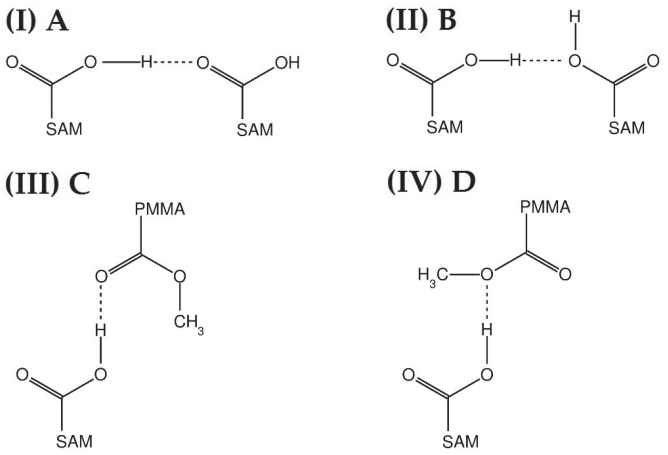

T a b l e 1. Average number of hydrogen bonds formed by the end groups of the COOH-terminated SAM

PMMA	None	Isotactic	Syndiotactic	Atactic
Type A	25%	20%	24%	21%
Type B	29%	26%	24%	26%
Type C	–	24%	22%	22%
Type D	–	2%	1%	2%
None	46%	28%	25%	29%

The time-averaged numbers of such bonds in all studied models of COOH-terminated SAMs, uncoated and coated with PMMA of different tacticity, are provided in Table 1.

The data in the table suggest that the observed effect cannot be attributed to differences in hydrogen bond formation with a COOH-terminated SAM by PMMA of different tacticity, as was hypothesized in [6]. The COOH groups which take part in bonding with PMMA are those which were previously not engaged or in a state of switching between acceptors, rather than those taking part in bonding between carboxylic groups.

The actual effect of interaction may be observed by plotting the time-averaged local μ_z/S vertical scan through the PMMA layer, along the vertical simulation box coordinate z. The value at a given point is computed as the net μ_z of a slice of the layer of a specific width, divided by the area perpendicular to the scan direction S. An exemplary chart obtained for a syndiotactic PMMA model on SAM–COOH showing the dependence of this quantity on the z coordinate for chosen slice heights is shown in Fig. 4.

Analysis should begin with values of z greater than *ca.* 36 Å. While for an infinitely large model the curves should be expected to be flat, for a finite size model structural features (*i.e.* chain fragments with a specific geometry) can be observed, resulting in fluctuations of the quantity of interest. The variation of the curves with slice height indicates that the non-zero value is incidental and depends on what structural features have been captured in the slice. However, below a z value of *ca.* 36 Å, the presence of a highly polarized structure within the PMMA directly at the interface with the SAM clearly manifests itself. The polarization peak increases with slice height up to a point where it does not vary further, determining the slice height which approximately captures the entire polarized structure. A summary of the computed values for all models is given in Table 2.

Analysis of the data in the table suggests that in principle, PMMA polarizes strongly at the interface with a COOH-terminated SAM and weakly at the interface with a CH_3-terminated SAM. Syndiotactic PMMA is slightly different in that it polarizes significantly also on the latter interface, despite CH_3 groups being less polar than COOH groups.

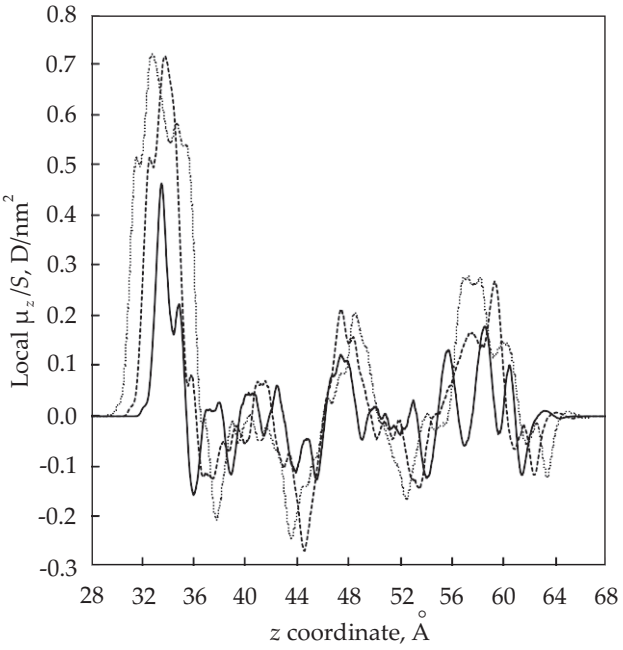

Fig. 4. Local vertical component of the dipole moment of a syndiotactic PMMA model deposited on a COOH-terminated SAM as a function of the vertical coordinate; solid line for a slice width of 1 Å, dashed for 3 Å and dotted for 5 Å

Comparison with experimental results

By subtracting the values of interfacial polarization at the interface with a CH_3-terminated SAM from the values at the interface with a COOH-terminated SAM, expected relative values $\Delta(\mu_z/S)$ were calculated and compared with the measurements by Marzec *et al*. [6]. The change in ΔV_{CPD} between the two types of SAMs caused by coating with PMMA can be transformed to a polarization value by use of Eq. (1).

For isotactic PMMA the effect measured in simulations was *ca.* +0.55 D/nm^2, while in experiments an effect of *ca.* +0.465 D/nm^2 was measured. This may be regarded as a very good agreement. For syndiotactic PMMA simulations yield +0.45 D/nm^2 and experiments *ca.* +0.4513 D/nm^2. While seemingly a perfect agreement, it should be noted that the simulation result may have a non-negligible uncertainty, since it varies slightly when repeating simulations. This effect is related to the finite size of the model. It is worth noting that coating with syndiotactic PMMA, in light of this result, has a similar effect to coating with isotactic PMMA only due to compensation of the increased polarization on both types of SAMs. Finally, for atactic PMMA a value of

T a b l e 2. Interfacial polarization of the polymer layer on top of the SAM in D/nm^2

SAM	SAM–CH_3			SAM–COOH		
PMMA	Isotactic	Syndiotactic	Atactic	Isotactic	Syndiotactic	Atactic
Polarization	+0.11	+0.41	+0.10	+0.66	+0.86	+0.78

ca. +0.68 D/nm^2 was obtained in simulations, while experiments yielded *ca*. +0.791 D/nm^2. This may be regarded as a good agreement, in spite of the fact that the polymer used in experiments was far from an ideal atactic one.

Mechanism of the interaction

The findings of the previous subchapter should be complemented with an analysis of how the observed polarization effect arises. Having located the exact area of interest, an analysis of the geometrical arrangements of individual mers at the PMMA-SAM interface was performed. Three recurring types of identified arrangements are presented in Fig. 5.

In syndiotactic and atactic systems, mirror images of these arrangements, L_1, L_2 and L_3, respectively, can be found as well. The oxygen atom closest to the SAM surface creates an opportunity for a hydrogen bond formation from a COOH group.

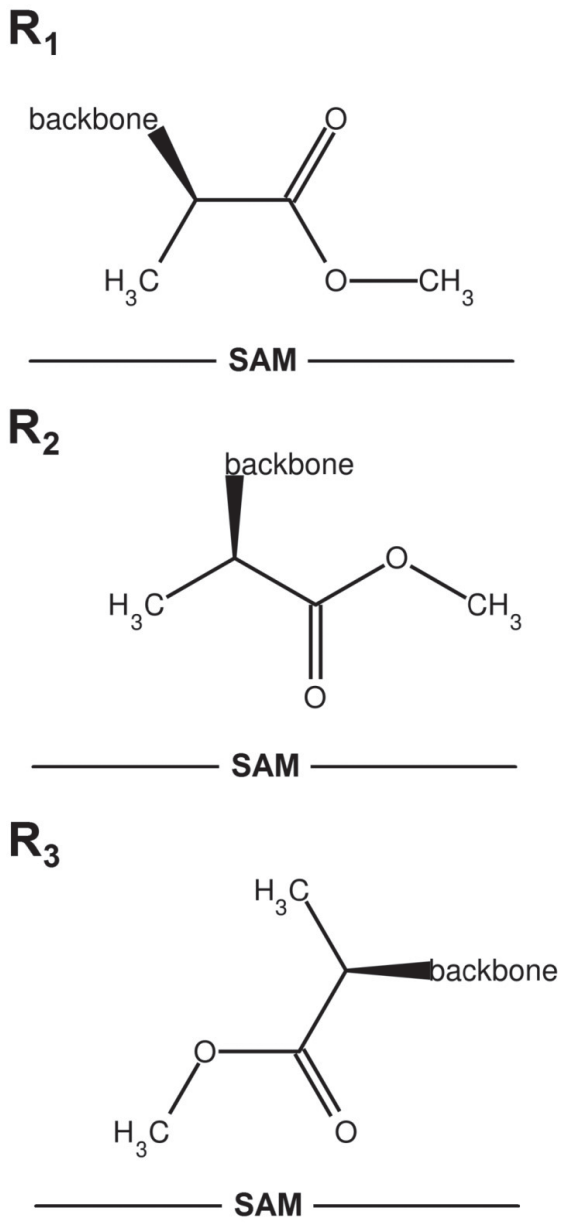

Fig. 5. Characteristic geometrical arrangements of PMMA mers on the COOH-terminated SAM interface

Individual PMMA mers have non-zero net electric dipole moments. Arrangements $R_1$and L_1 have a negative vertical component of the dipole moment, while the other have a positive component. A more frequent occurrence of the latter arrangements explains why the observed polarization has a positive sign.

A study of the interface also revealed that the above described arrangements often occur in various sequences where an individual PMMA macromolecule fragment is located close to the interface. Short isotactic triads containing a mix of R_2 and R_3 arrangements occurred frequently in models in which the highest polarization values were observed. However, they were observed more frequently in atactic and mixed tacticity models than in a purely isotactic one, suggesting that short isotactic sequences need to be separated by syndiotactic or heterotactic sequences along the chain to produce a strong effect. This may occur in atactic and eutactic systems. Additionally, in syndiotactic PMMA, tetrads in which R_2 or R_3 is separated by two mers twisted away from the interface from L_2 or L_3 were observed and were significant contributors to the polarization, regardless of SAM type. This suggests that syndiotactic sequences are flexible enough to also contribute significantly to the effect. The existence of an optimal (for yielding an even stronger effect) eutactic polymer with a mix of syndiotactic and isotactic sequences along the chain can be hypothesized, but in reality could be impossible to synthesize. For this reason searches for such sequence were abandoned and results of attempts at it are not presented in this work.

Additional considerations

While the thickness of the PMMA layers in the MD models is much smaller than can possibly be obtained in samples prepared for experiments, the observed effect is strictly limited to the interface between the polymer and the SAM. This suggests that the simulated layer only needs to be thick enough to reliably model part of the bulk polymer above the layer. The implied independence of the observed effect on the polymer layer thickness in simulations is in agreement with the findings of [6], where it is shown that the measured effect for an atactic polymer is largely independent of the layer thickness.

The cited paper [6] includes several interesting speculations on explaining the effect, most of which should be clarified by this work. However, the authors consider also a possibility of protonation of PMMA mers caused by dissociation of COOH groups upon contact with the organic solvent. If this effect occurred at any significant rate (more than 1% of the COOH groups dissociating and causing a protonation event), the resulting contribution to the vertical component of the net electric dipole moment of the system would exceed the highest values observed in simulations and experiments. Therefore it

must be assumed that this does not occur at any significant rate at all or is a largely reversible effect.

CONCLUSIONS

To summarize, in this work models of self-assembled monolayers formed by hexadecanethiol and 1-mercapto hexadecanoic acid were prepared. The models, containing a total of 400 molecules deposited on a five layer model of the (111) surface of gold, were coated with models of poly(methyl methacrylate) of different tacticity. The PMMA models consisted of 12 chains of 150 mers each and were forced into an amorphous structure in a "die casting" simulation. The result of interaction was a geometrical organization of individual PMMA mers at the interface with the SAM, leading to a polarization of the polymer at the interface. The effect was observed to be generally stronger for a COOH-terminated SAM due to a higher polarity of its end groups, resulting in stronger electrostatic interaction. Fine details of this effect are different for PMMA of different tacticity, but mixed tacticity systems, including atactic ones, generally lead to a stronger polarization on top of a COOH-terminated SAM compared to a CH_3-terminated SAM.

The conclusions of this work are that SAMs are largely unaffected by deposition of a PMMA layer and it is the polymer layer itself that is affected by the interaction. Specifically, the layer becomes polarized exactly at the interface. As this effect appears to be highly sensitive to the local tacticity structure of the chain, applications of PMMA layers to further fine-tuning of the work function of the entire structure are limited, as the observed effect may greatly depend on how well the tacticity can be controlled in the synthesis process, if at all.

This work was supported by the Polish Ministry of Science and Higher Education and its grants for Scientific Research.

REFERENCES

[1] Vericat C., Vela M.E., Benitez G. *et al.*: *Chemical Society Review* **2010**, *39*, 1805. https://doi.org/10.1039/B907301A
[2] Lee J.W., Sim S.J., Cho S.M., Lee J.: *Biosensors and Bioelectronic* **2005**, *20*, 1422. http://dx.doi.org/10.1016/j.bios.2004.04.017
[3] Sushko M.L., Shluger A.L.: *Journal of Physics and Chemistry B* **2007**, *111*, 4019. https://doi.org/10.1021/jp0688557
[4] Sushko M.L., Schluger A.L.: *Advanced Functional Materials* **2008**, *18*, 2228. https://doi.org/10.1002/adfm.200701305
[5] Sushko M.L., Shluger A.L.: *Advanced Materials* **2009**, *21*, 1111. https://doi.org/10.1002/adma.200801654
[6] Marzec M.M., Awsiuk K., Dąbczyński P. *et al.*: *Macromolecular Chemistry and Physics* **2018**, *219*, 1800097. https://doi.org/10.1002/macp.201800097
[7] Berendsen H.J.C., van der Spoel D., van Drunen R.: *Computer Physics Communications* **1995**, *91*, 43. https://doi.org/10.1016/0010-4655(95)00042-E
[8] Lindahl E., Hess B., van der Spoel D.: *Journal of Molecular Modeling* **2001**, *7*, 306. http://dx.doi.org/10.1007/s008940100045
[9] van der Spoel D., Lindahl E., Hess B. *et al.*: *Journal of Computational Chemistry* **2005**, *26*, 1701. http://dx.doi.org/10.1002/jcc.20291
[10] Hess B., Kutzner C., van der Spoel D., Lindahl E.: *Journal of Chemical Theory and Computation* **2008**, *4*, 435. https://doi.org/10.1021/ct700301q
[11] Pronk S., Pall S., Schulz R. *et al.*: *Bioinformatics* **2013**, *29*, 845. http://dx.doi.org/10.1093/bioinformatics/btt055
[12] Abraham M.J., Murtola T., Schulz R. *et al.*: *SoftwareX* **2015**, *1*, 19. https://doi.org/10.1016/j.softx.2015.06.001
[13] Jorgensen W.L., Tirado-Rives J.: *Journal of American Chemical Society* **1988**, *110*, 1657. https://doi.org/10.1021/ja00214a001
[14] Jorgensen W.L., Maxwell D.S., Tirado-Rives J.: *Journal of American Chemical Society* **1996**, *118*, 11225. https://doi.org/10.1021/ja9621760
[15] Jorgensen W.L., McDonald N.A.: *Journal of Molecular Structure: THEOCHEM* **1998**, *424*, 145. https://doi.org/10.1016/S0166-1280(97)00237-6
[16] McDonald N.A., Jorgensen W.L.: *Journal of Physics and Chemistry B* **1998**, *102*, 8049. https://doi.org/10.1021/jp981200o
[17] Rizzo R.C., Jorgensen W.L.: *Journal of American Chemical Society* **1999**, *121*, 4827. https://doi.org/10.1021/ja984106u
[18] Price M.L.P., Ostrovsky D., Jorgensen W.L.: *Journal of Computational Chemistry* **2001**, *22*, 1340. https://doi.org/10.1002/jcc.1092
[19] Watkins E.K., Jorgensen W.L.: *Journal of Physics and Chemistry A* **2001**, *105*, 4118. https://doi.org/10.1021/jp004071w
[20] Kaminski G., Friesner R.A., Tirado-Rives J., Jorgensen W.L.: *Journal of Physics and Chemistry B* **2001**, *105*, 6474. https://doi.org/10.1021/jp003919d
[21] Hohenberg P., Kohn W.: *Physical Review Journals Archive* **1964**, *136 (3B)*, B864. https://doi.org/10.1103/PhysRev.136.B864
[22] Kohn W., Sham L.J.: *Physical Review Journals Archive* **1965**, *140 (4A)*, A1133. https://doi.org/10.1103/PhysRev.140.A1133
[23] https://www.basissetexchange.org/ (accessed 15.03.2020).
[24] Becke A.D.: *Physical Review A* **1988**, *38*, 3098. https://doi.org/10.1103/PhysRevA.38.3098
[25] Lee C., Yang W., Parr R.G.: *Physical Review B* **1988**, *37*, 785.

https://doi.org/10.1103/PhysRevB.37.785
[26] Valiev M., Bylaska E.J., Govind N. *et al*.: *Computer Physics Communications* **2010**, *181*, 1477. https://doi.org/10.1016/j.cpc.2010.04.018
[27] Humphrey W., Dalke A., Schulten K.: *Journal of Molecular Graphics* **1996**, *14*, 33. https://doi.org/10.1016/0263-7855(96)00018-5
[28] Zhang L., Goddard W.A., Jiang S.: *The Journal of Chemical Physics* **2002**, *117*, 7342. https://doi.org/10.1063/1.1507777
[29] Ulman A., Eilers J.E., Tillman N.: *Langmuir* **1989**, *5*, 1147. https://doi.org/10.1021/la00089a003
[30] Lincoln R.C., Koliwad K.M., Ghate P.B.: *Physical Review Journals Archive* **1967**, *157*, 463. https://doi.org/10.1103/PhysRev.157.463
[31] Darden T., York D., Pedersen L.: *The Journal of Chemical Physics* **1993**, *98*, 10089. https://doi.org/10.1063/1.464397
[32] Essmann U., Perera L., Berkowitz M.L.: *The Journal of Chemical Physics* **1995**, *103*, 8577. https://doi.org/10.1063/1.470117
[33] Pall S., Hess B.: *Computer Physics Communications* **2013**, *184*, 2641. https://doi.org/10.1016/j.cpc.2013.06.003
[34] Feenstra P., Brunsteiner M., Khinast J.: *International Journal of Pharmaceutics* **2012**, *431*, 26. https://doi.org/10.1016/j.ijpharm.2012.03.049
[35] Mortazavian H., Fennell C.J., Blum F.D.: *Macromolecules* **2016**, *49*, 4211. https://doi.org/10.1021/acs.macromol.5b02214

Received 17 III 2020.

W kolejnym zeszycie ukażą się m.in. następujące artykuły:

J. Paciorek-Sadowska, M. Borowicz, M. Isbrandt, Ł. Grzybowski, B. Czupryński – Zastosowanie biodegradowalnego polimeru jako alternatywnego surowca do produkcji nowego ekopoliolu

P. Kasprzyk, K. Błażek, P. Parcheta, J. Datta – *Zielone* termoplastyczne elastomery poli(etero-uretanowe) – synteza i badania struktury chemicznej oraz wybranych właściwości (*j. ang.*)

L. Szczepkowski, J. Ryszkowska, M. Auguścik-Królikowska, M. Leszczyńska, A. Przekurat, S. Przekurat – Nowe addukty amin z ditlenkiem węgla jako porofory w produkcji integralnych pianek poliuretanowych (*j. ang.*)

A. Strąkowska, S. Członka, K. Miedzińska, K. Strzelec – Sztywne pianki poliuretanowe o właściwościach antybakteryjnych modyfikowane olejkiem sosnowym (*j. ang.*)

K. Uram, A. Prociak, M. Kurańska – Wpływ struktury chemicznej biopolioli z oleju rzepakowego na wybrane właściwości pianek poliuretanowych (*j. ang.*)

M. Auguścik-Królikowska, J. Ryszkowska, A. Ambroziak, L. Szczepkowski, R. Oliwa, M. Oleksy – Struktura i właściwości lepkosprężystych pianek poliuretanowych napełnionych fusami kawy (*j. ang.*)

M. Kirpluks, A. Ivdre, A. Fridrihsone, U. Cabulis – Sztywne pianki poliuretanowe na bazie oleju talowego napełnione nanofibrylarną celulozą (*j. ang.*)

M. Leszczyńska, J. Ryszkowska, L. Szczepkowski – Kompozyty sztywnych pianek poliuretanowych z łupinami orzechów (*j. ang.*)